Supporting Information:
Mean-field models for the chemical fueling of transient soft matter states

Sven Pattloch[1,2] and Joachim Dzubiella[1,2]

[1] *Applied Theoretical Physics - Computational Physics, Physikalisches Institut, Albert-Ludwigs-Universität Freiburg, D-79104 Freiburg, Germany*
[2] *Cluster of Excellence livMatS @ FIT - Freiburg Center for Interactive Materials and Bioinspired Technologies, Albert-Ludwigs-Universität Freiburg, D-79110 Freiburg, Germany*

(Dated: August 30, 2023)

DERIVATION OF $F_{\max}$

For the evaluation of

$$\begin{aligned} Z_{\max} &= \int_{-\infty}^{\infty} e^{-\mathcal{H}_{\mathrm{sym}}} \mathrm{d}Q \\ &= \int_{-\infty}^{\infty} e^{-(AQ^2+BQ^4)} \mathrm{d}Q \\ &= 2\int_{0}^{\infty} e^{-AQ^2-BQ^4} \mathrm{d}Q \end{aligned} \tag{S1}$$

we start with the substitution $u = \sqrt{B}Q^2 + \frac{A}{2\sqrt{B}}$:

$$\begin{aligned} Z_{\max} &= \int_{-\infty}^{\infty} e^{-AQ^2-BQ^4} \mathrm{d}Q \\ &= e^{\frac{A^2}{4B}} \frac{1}{B^{1/4}} \int_{\frac{A}{2\sqrt{B}}}^{\infty} e^{-u^2} \frac{1}{\sqrt{u - \frac{A}{2\sqrt{B}}}} \mathrm{d}u \end{aligned} \tag{S2}$$

Note, that we replaced ΔQ by Q for better readability. Because of infinite integration boundaries the shift by Q_{c} does not affect the integrals value. Now we just need to apply the formula

$$\begin{aligned} \int_{-c}^{\infty} \frac{e^{-x^2}}{\sqrt{x+c}} \mathrm{d}x &= \frac{\sqrt{-c}e^{-c^2/2}}{\sqrt{2}} \int_{0}^{\infty} e^{-\frac{c^2}{2}\cosh(t)} \cosh\left(\frac{t}{4}\right) \mathrm{d}t \\ &= \frac{\sqrt{-c}e^{-c^2/2} K_{\frac{1}{4}}\left(\frac{c^2}{2}\right)}{\sqrt{2}} \end{aligned} \tag{S3}$$

where K is the modified Bessel function of the second kind with its corresponding integral representation. For its derivation, we need the substitution $v = \sqrt{2}\sinh\left(\frac{t}{4}\right)$ and the relation $\cosh(t) = 2\cosh^2\left(\frac{t}{2}\right) - 1 = 2\left(2\sinh^2\left(\frac{t}{4}\right) + 1\right)^2 - 1$. In total, we obtain

$$Z_{\max} = e^{\frac{A^2}{8B}} \frac{K_{\frac{1}{4}}\left(\frac{A^2}{8B}\right)}{2\sqrt{-\frac{B}{A}}} \tag{S4}$$

where only the logarithm has to be taken in order to obtain $F_{\max}$.

NUMERICAL DETAILS OF FITTING

For having a quantitative measure of the fit quality we introduce χ^2 as the sum over the squared errors between actual data points and corresponding fitting value. Let (t_{ijk}, R_{ijk}) be the experimental data points (denoting time and radius). The index i runs over the considered pH-values 6.1 and 7.2, respectively, j over the initial fuel concentrations used for pH i and k is just the kth point in this set. In total, we have the sum

$$\chi^2 = \sum_{ijk} \left(f\left(t_{ijk}\right) - R_{ijk}\right)^2 \tag{S5}$$

where f maps the time t_{ijk} to the radius R determined by our equations in the quasistatic case.

The fits are executed using the python package *lmfit* [1], which is based on *scipy.optimize* [2]. They use an Levenberg–Marquardt algorithm [3, 4] in order to find the MSD. Essentially, we define the function which calculates the radii in dependency of time, initial fuel concentration and fitting parameters. By applying *lmfit*, it takes this function as well as the experimental data and then minimizes the MSD between experiment and model.

	pH = 6.1	pH = 7.2
$A\ \left[k_{\mathrm{B}}T\,\mathrm{nm}^{-2}\right]$	-2.20×10^{-4}	-1.18×10^{-4}
$B\ \left[k_{\mathrm{B}}T\,\mathrm{nm}^{-4}\right]$	6.07×10^{-9}	1.75×10^{-9}
Q_{c} [nm]	402	341
$m\ \left[k_{\mathrm{B}}T\,\mathrm{l\,mmol}^{-1}\mathrm{nm}^{-1}\right]$	8.57×10^{-2}	0.156
$\tilde{k}_+\ \left[\mathrm{l\,mmol}^{-1}\mathrm{h}^{-1}\right]$	27.9	14.4
$k_-\ \left[\mathrm{h}^{-1}\right]$	2.07×10^{-2}	5.75×10^{-2}
$p_{\mathrm{sat}}\ \left[\mathrm{mmol\,l}^{-1}\right]$	0.799	
$p^*\ \left[\mathrm{mmol\,l}^{-1}\right]$	0.530	0.768
$k_+ = \tilde{k}_+ p_{\mathrm{sat}}\ \left[\mathrm{h}^{-1}\right]$	22.3	11.5
$Q_1 = Q_{\mathrm{c}} - \sqrt{-A/2B}$ [nm]	267	157
$Q_2 = Q_{\mathrm{c}} + \sqrt{-A/2B}$ [nm]	537	525

TABLE SI: Fit values with pH-dependent parameters for the energy landscape belonging to Fig. S1

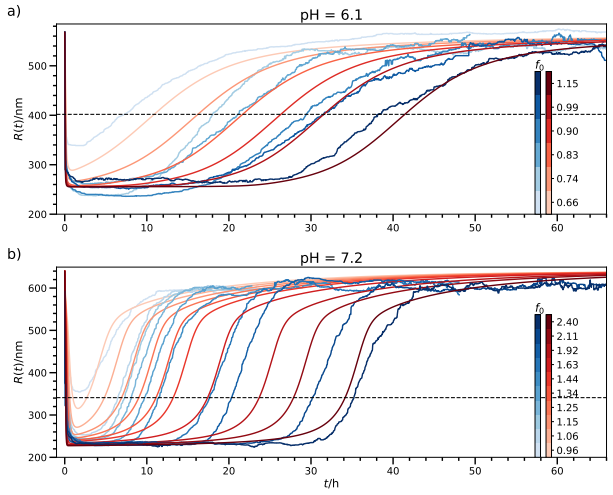

FIG. S1: Fit where the energy landscape parameters (A, B, Q_c) are not global but also pH-dependent, corresponding values can be found in Tab. SI in this ESI. By adjusting the energy landscape for each pH value we better hit the plateau values; $\chi^2 = 1.944 \cdot 10^7$

	pH = 6.1	pH = 7.2
$A\ [k_\mathrm{B}T\,\mathrm{nm}^{-2}]$	-3.87×10^{-4}	
$B\ [k_\mathrm{B}T\,\mathrm{nm}^{-4}]$	7.50×10^{-9}	
Q_c [nm]	391	
$m\ [k_\mathrm{B}T\,\mathrm{l\,mmol}^{-1}\mathrm{nm}^{-1}]$	4.72×10^{-2}	0.274
$\tilde{k}_+\ [\mathrm{l\,mmol}^{-1}\mathrm{h}^{-1}]$	25.6	14.4
$k_-\ [\mathrm{h}^{-1}]$	2.07×10^{-2}	5.61×10^{-2}
$p_\mathrm{sat}\ [\mathrm{mmol\,l}^{-1}]$	0.799	
$p^*\ [\mathrm{mmol\,l}^{-1}]$	0.545	0.761
$k_+ = \tilde{k}_+ p_\mathrm{sat}\ [\mathrm{h}^{-1}]$	20.4	11.5
$Q_1 = Q_\mathrm{c} - \sqrt{-A/2B}$ [nm]	230	
$Q_2 = Q_\mathrm{c} + \sqrt{-A/2B}$ [nm]	551	

TABLE SII: Fitting values for an energy barrier of $5\,k_\mathrm{B}T$, see Fig. S6

ALTERNATIVE FITS

In this and the following sections, we show fits similar to Fig. 3 in the main paper but with small variations.

pH-dependent energy landscape

In Fig. S1 we show a fit where the energy landscape parameters (A, B, Q_c) are not global but also pH-dependent, corresponding values can be found in Tab. SI in this ESI.

Unimodal Hamiltonian of form Q^2 and Q^4

For $B = 0$ we have the reduced Hamiltonian

$$\mathcal{H}(Q,t) = A(\Delta Q)^2 + m \cdot (p(t) - p^*)\,\Delta Q \qquad \text{(S6)}$$

which has only one local minimum for $A > 0$. The mean radius $\langle R \rangle$ is predominately determined by this minimum at

$$\begin{aligned} H' &= 2A\,(Q - Q_\mathrm{c}) + m\,(p - p^*) \overset{!}{=} 0 \\ \Rightarrow Q_\mathrm{min} &= Q_\mathrm{c} - \frac{m\,(p - p^*)}{2A} \end{aligned} \qquad \text{(S7)}$$

because the small asymmetry by the linear term has no significant effects. This means, that the mean radius depends linearly on the concentration. Since the shape of $p\,(t)$ deviates from the experiments, we will never have congruent fits.
Note that the position of the minimum does not change when we multiply A and m with the same factor. Hence, the fitting algorithms create energy landscapes leading to overflows. This means, we have to fix one of these values in order to carry out a fit. In our case, we fixed $A = 0.0001$

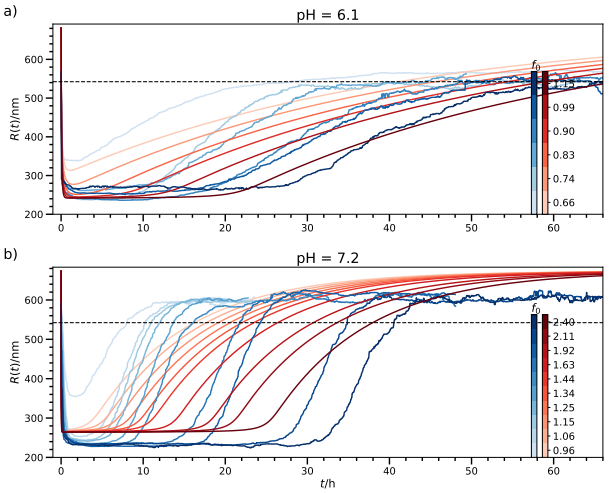

FIG. S2: Alternative fit with an unimodal potential (values see Tab III). The model can't replicate the fast transitions from one state to the other so that it is cheaper with respect to χ^2 to use to high plateau values; $\chi^2 = 7.333 \cdot 10^7$

The same issues are observed for an unimodal Q^4 form.

Unimodal Hamiltonian of form Q^6

Compared to the quadratic Hamiltonian from eq. S6, we can improve our fits by a higher order potential such

	pH = 6.1	pH = 7.2
A $[k_\mathrm{B}T\,\mathrm{nm}^{-2}]$	1.00×10^{-4}	
B $[k_\mathrm{B}T\,\mathrm{nm}^{-4}]$	0.00	
Q_c [nm]	542	
m $[k_\mathrm{B}T\,\mathrm{l\,mmol}^{-1}\mathrm{nm}^{-1}]$	0.115	0.107
$\tilde{k}_+$ $[\mathrm{l\,mmol}^{-1}\mathrm{h}^{-1}]$	23.2	30.1
$\tilde{k}_+ p_\mathrm{sat}$ $[\mathrm{h}^{-1}]$	5.61	7.39
k_- $[\mathrm{h}^{-1}]$	2.46×10^{-2}	8.65×10^{-2}
p_sat $[\mathrm{mmol\,l}^{-1}]$	0.768	
p^* $[\mathrm{mmol\,l}^{-1}]$	0.242	0.245

TABLE SIII: Fit values for the quadratic potential (see Fig. S2). $A = 0.0001$ was fixed

	$pH = 6.1$	$pH = 7.2$
A $[k_\mathrm{B}T\,\mathrm{nm}^{-2}]$	0.00	
B $[k_\mathrm{B}T\,\mathrm{nm}^{-4}]$	6.09×10^{-14}	
Q_c [nm]	379	
m $[k_\mathrm{B}T\,\mathrm{l\,mmol}^{-1}\mathrm{nm}^{-1}]$	0.168	0.602
$\tilde{k}_+$ $[\mathrm{l\,mmol}^{-1}\mathrm{h}^{-1}]$	28.2	11.1
k_- $[\mathrm{h}^{-1}]$	2.10×10^{-2}	6.17×10^{-2}
p_sat $[\mathrm{mmol\,l}^{-1}]$	0.768	
p^* $[\mathrm{mmol\,l}^{-1}]$	0.558	0.721
$\tilde{k}_+ p_\mathrm{sat}$ $[\mathrm{h}^{-1}]$	15.7	8.01

TABLE SIV: Fit values for the Q^6 potential (see Fig. S3)

as

$$\mathcal{H}(Q,t) = A(\Delta Q)^6 + m \cdot (p(t) - p^*)\,\Delta Q. \qquad \text{(S8)}$$

The resulting fits and its corresponding values can be found in Fig. S3 and Tab. SIV, respectively. Measured by χ^2 the fits quality is still worse than the quartic form, but the difference shrinks. However, this potential is very flat as one can see in Fig. S4 leading to another problem. Now the particles size distribution is very broad. Especially in the symmetric case, we find a significant amount of particles ranging from radii 200 nm up to 600 nm while we see relatively sharp distributions in the experimental data.

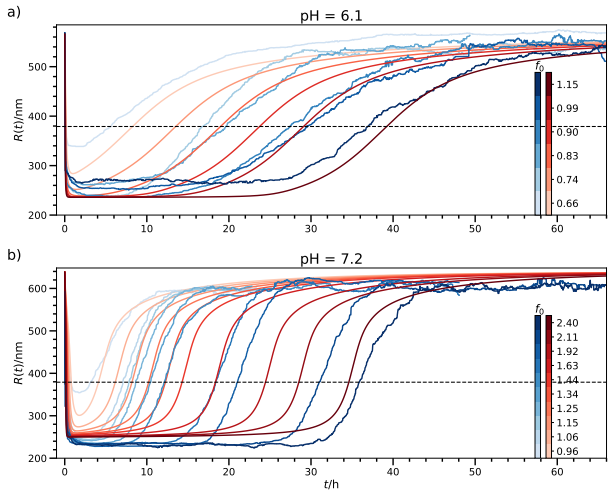

FIG. S3: Same as Fig. S2 but with a Q^6 potential (values see Tab. SIV). Now the transitions are better met, but the size distribution of the colloids is still not satisfactory; $\chi^2 = 2.4 \cdot 10^7$

Box potential

We also tested a completely different potential, namely a box potential. Therefore, we introduce new parameters

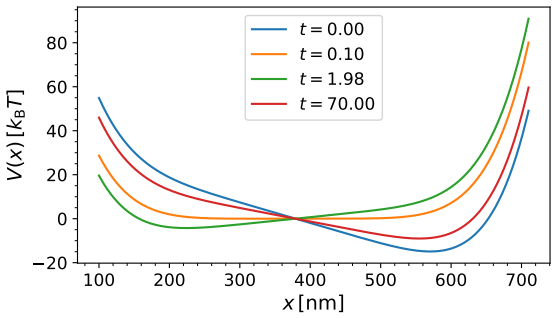

FIG. S4: Potential of the Q^6 potential of Fig. S3. Obviously the potential is extremely flat over a wide span of radii leading to a broad size distribution

$Q_\mathrm{left/right}$ representing the endpoints of the box. Thus, we obtain a Hamiltonian

$$\mathcal{H}(Q,t) = \begin{cases} m \cdot (p(t) - p^*)\,Q, & Q_\mathrm{left} \le Q \le Q_\mathrm{right} \\ \infty, & \text{else} \end{cases}. \qquad \text{(S9)}$$

The resulting fit shown in Fig. S5 is very close to the bimodal one, but again we find some concerns regarding the size distribution. When $p > p^*$ the minimum of the distribution is at Q_left so that most of the colloids are in this state. With 177 nm its value is already below the value $R_\mathrm{H,z} = 206\,\mathrm{nm}$ of the core-shell particles before acidic cleavage which we assume as a lower boundary of the microgels radii.

Fitting with other barrier height

In Fig. S6 we show a fit with a barrier height of $5\,k_\mathrm{B}T$ instead of $2\,k_\mathrm{B}T$, corresponding values can be found in Tab. SII

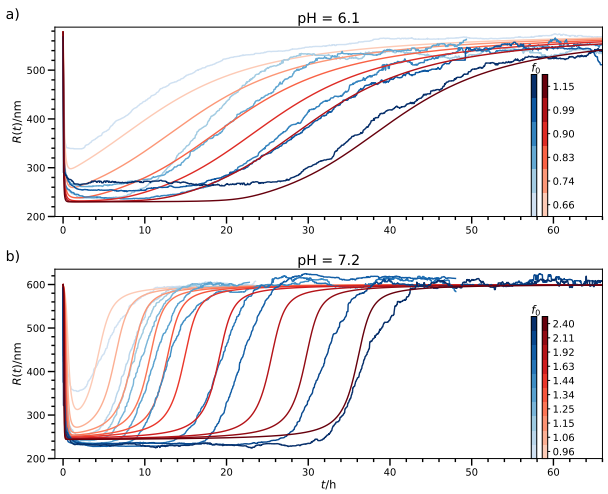

FIG. S5: Alternative fit with a box potential (values see Tab V). In general we have a good fit quality, but the size distribution of the colloids is questionable at some point; $\chi^2 = 2.2 \cdot 10^7$

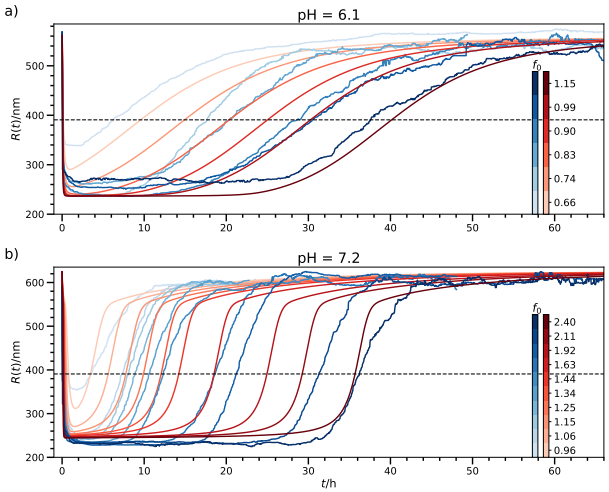

FIG. S6: Alternative fit with a barrier height of $5\,k_\mathrm{B}T$, corresponding values can be found in Tab. SII; $\chi^2 = 2.189 \cdot 10^7$

	$pH = 6.1$	$pH = 7.2$
Q_left [nm]	177	
Q_right [nm]	604	
m $\left[k_\mathrm{B}T\,\mathrm{l\,mmol^{-1}nm^{-1}}\right]$	6.97×10^{-2}	0.286
$\tilde{k}_+$ $\left[\mathrm{l\,mmol^{-1}h^{-1}}\right]$	23.6	12.1
k_- $\left[\mathrm{h^{-1}}\right]$	2.03×10^{-2}	5.51×10^{-2}
p_sat $\left[\mathrm{mmol\,l^{-1}}\right]$	0.822	
p^* $\left[\mathrm{mmol\,l^{-1}}\right]$	0.548	0.768
$\tilde{k}_+ p_\mathrm{sat}$ $\left[\mathrm{h^{-1}}\right]$	12.9	9.32

TABLE SV: Fit values for a box potential (see Fig. S5). $Q_\mathrm{left/right}$ are free fit parameters and represent the boundaries if the box

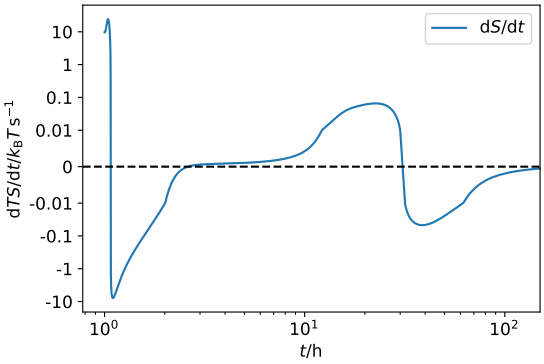

FIG. S7: Time derivative of entropy shown in Fig. 6a of the main paper.

ENTROPY PRODUCTION

Fig. S7 shows the time derivative of the entropy, i.e., the entropy production. Larger changes occur at the transition points from swollen to collapsed an vice versa. We see that during the first transition the absolute values of dS are order of magnitudes larger in a short time span when compared to the transition at later times. While the colloids are collapsed the entropy production is almost vanishing.

THERMODYNAMIC PLOTS WITH LOGARITHMIC TIME-AXIS

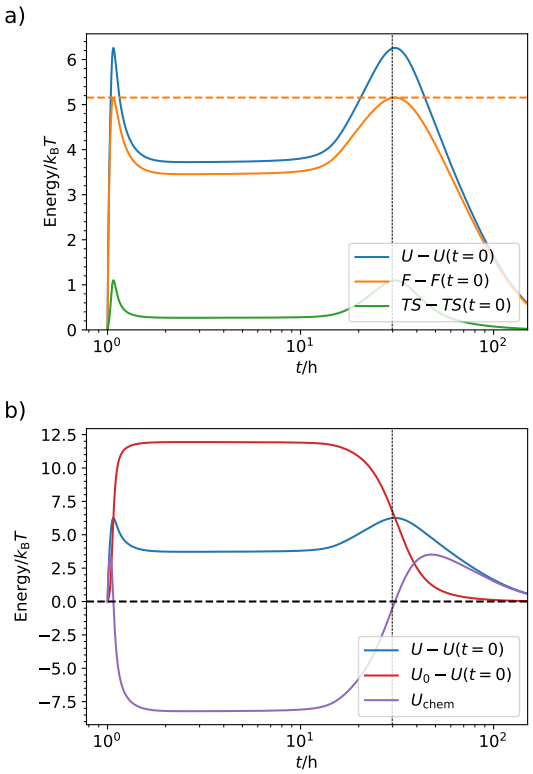

FIG. S8: Same as Fig. 6 in the main manuscript but now with logarithmic time-axes.The time-dependent energetics of the first transition at short times can be better viewed in this plot.

DEFINITION OF THE KRAMERS TIME

In Fig. S9 one can see a plot analogous to Fig. 7 of the main paper but with an alternative definition of the Kramers time

$$\tau_{\text{Kramers}} = \frac{2\pi}{\beta D}\left[\mathcal{H}''\left(Q_{\max}\right)\mathcal{H}''\left(Q_{\min,\text{right}}\right)\right]^{1/2} e^{\beta\Delta\mathcal{H}} \tag{S10}$$

taking into account the curvatures of the energy landscape at the maximum and the right minimum, respectively. Because the positions of the minima depend on time, we consistently use the values for the time where the energy landscape is symmetric. Comparing both timescales we see that they differ by less than a factor of 2 meaning that both are suitable for time scale estimations. We chose the definition of the main paper because of its properties in the limit of vanishing barriers. Then, our definition equals the time needed for pure diffusion from the minimum to the barrier.

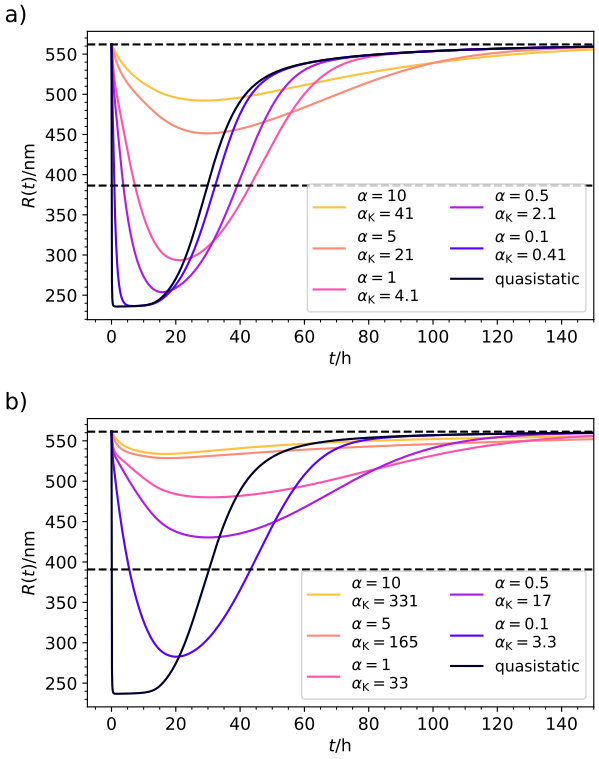

FIG. S9: Same as Fig. 7 in the main paper but the Kramers time is defined according to eq. (S10).

[1] M. Newville, T. Stensitzki, D. B. Allen, and A. Ingargiola, "LMFIT: Non-Linear Least-Square Minimization and Curve-Fitting for Python," (2014).

[2] P. Virtanen, R. Gommers, T. E. Oliphant, M. Haberland, T. Reddy, D. Cournapeau, E. Burovski, P. Peterson, W. Weckesser, J. Bright, S. J. van der Walt, M. Brett, J. Wilson, K. J. Millman, N. Mayorov, A. R. J. Nelson, E. Jones, R. Kern, E. Larson, C. J. Carey, İ. Polat, Y. Feng, E. W. Moore, J. VanderPlas, D. Laxalde, J. Perktold, R. Cimrman, I. Henriksen, E. A. Quintero, C. R. Harris, A. M. Archibald, A. H. Ribeiro, F. Pedregosa, P. van Mulbregt, and SciPy 1.0 Contributors, Nature Methods **17**, 261 (2020).

[3] K. Levenberg, Quarterly of Applied Mathematics **2**, 164 (1944).

[4] D. W. Marquardt, Journal of the Society for Industrial and Applied Mathematics **11**, 431 (1963).